RESEARCH ARTICLE

NANO · MICRO small
www.small-journal.com

Flexible Triboelectric Nanogenerator Patch for Accelerated Wound Healing Through the Synergy of Electrostimulation and Photothermal Effect

Zhuo Wang, Quanhong Hu, Shuncheng Yao, Shaobo Wang, Xi Liu, Cuiping Zhang,* Zhong Lin Wang,* and Linlin Li**

Physiological wound healing process can restore the functional and structural integrity of skin, but is often delayed due to external disturbance. The development of methods for promoting the repair process of skin wounds represents a highly desired and challenging goal. Here, a flexible, self-powered, and multifunctional triboelectric nanogenerator (TENG) wound patch (e-patch) is presented for accelerating wound healing through the synergy of electrostimulation and photothermal effect. To fabricate the triboelectric e-patch, a flexible and conductive hydrogel with a dual network of polyacrylamide (PAM) and polydopamine (PDA) is synthesized and doped with multi-walled carbon nanotubes (MCNTs). The hydrogel exhibits high conductivity, good stretchability, and high biocompatibility. The triboelectric e-patch assembled from the hydrogel can detect mechanical and electrical signals of human motions in a real-time manner. In a rodent model of full-thickness dorsal skin wound, the e-patch integrating self-driven electrostimulation and photothermal effect under the near-infrared light irradiation efficiently promotes wound repair and hair follicle regeneration through relieving inflammation, fastening collagen deposition, vascular regeneration, and epithelialization. It offers a promising way to accelerate wound healing.

1. Introduction

As the largest organ in the body, the skin is the first protective barrier of body to defense invasive pathogens and damages. Skin wounds caused by accidents, bacterial infections and diseases can easily turn into chronic, non-healing wounds and lose sensory and protective function.[1–7] Traditional bandages can physically protect the wound but display limited bioactivities and are insufficient for promoting the wound healing process.[8] Recently, emerging bandages, such as hydrogel-based ones, have received widespread attention, due to their unique flexibility and softness, high water content, and excellent biocompatibility.[3] However, there remains an urgent need for functional patches capable of monitoring wound microenvironment such as temperature in real-time, and promoting wound healing effectively.

More than a century ago, current passing through a human dermal wound was first observed.[9] The existence of endogenous electric fields (EFs) and their essential roles for tissue remodeling have been verified by numerous investigations in a variety of tissues.[10] EFs can modulate re-epithelialization process for dermal wound through directing the migration of wound-related cells, including epithelial cells and fibroblasts.[11,12] Based on this, functional devices with electrical stimulations (ESs) that provided a stronger electric field than the EFs have been developed and applied for promoting skin regeneration.[11,13] However, traditional devices for providing ESs are always cumbersome and clumsy, making them

Z. Wang, Z. L. Wang, L. Li
Guangzhou Institute of Blue Energy
Knowledge City
Huangpu District, Guangzhou 510555, P. R. China
E-mail: zhong.wang@mse.gatech.edu; lilinlin@binn.cas.cn

Z. Wang, Q. Hu, S. Yao, S. Wang, X. Liu, Z. L. Wang, L. Li
Beijing Key Laboratory of Micro-Nano Energy and Sensor
Center for High-Entropy Energy and Systems
Beijing Institute of Nanoenergy and Nanosystems
Chinese Academy of Sciences
Beijing 101400, P. R. China
E-mail: liuxipla@163.com

The ORCID identification number(s) for the author(s) of this article can be found under https://doi.org/10.1002/smll.202409756

DOI: 10.1002/smll.202409756

Q. Hu, S. Wang, L. Li
Center on Nanoenergy Research
Guangxi Colleges and Universities Key Laboratory of Blue Energy and Systems Integration
School of Physical Science & Technology
Guangxi University
Nanning 530004, P. R. China

X. Liu, C. Zhang
Medical Innovation Research Department
PLA General Hospital and PLA Medical College
Beijing 100048, P. R. China
E-mail: zcp666666@sohu.com

L. Li
School of Nanoscience and Technology
University of Chinese Academy of Sciences
Beijing 100049, P. R. China

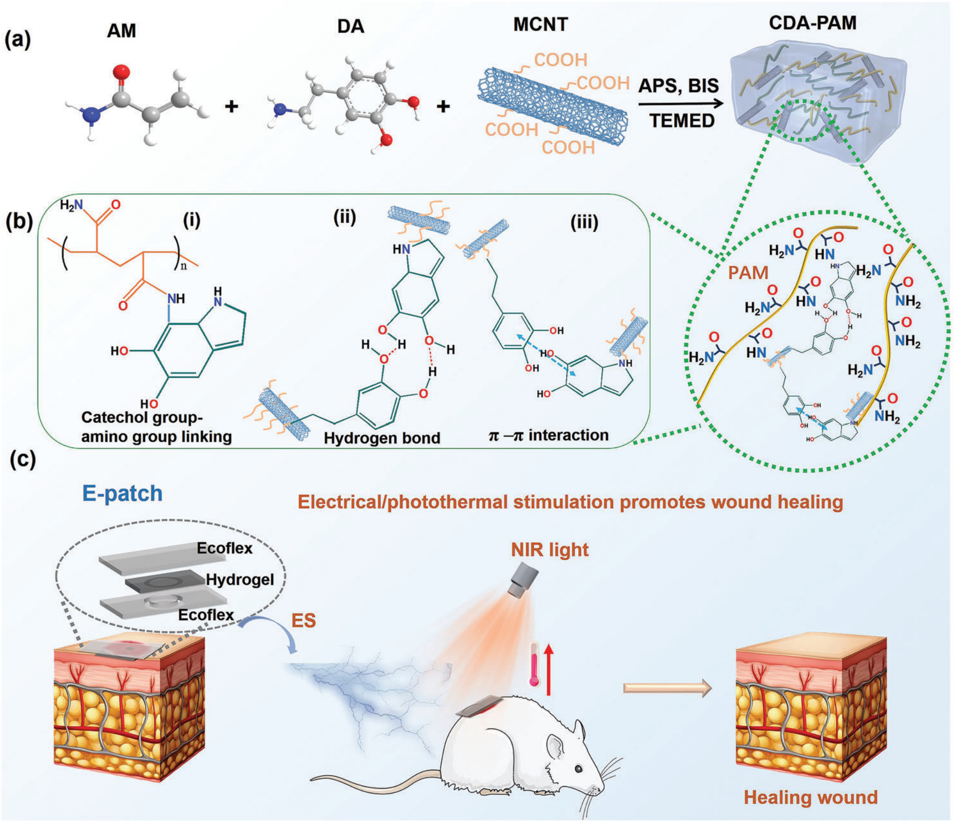

Scheme 1. Schematic diagram demonstrating the preparation process of the hydrogel and the applications of the hydrogel-based TENG e-patch for the promotion of wound healing. a) Schematic diagram of the preparation process of the CDA-PAM hydrogel. b) The chemical interaction of the hydrogel and schematic illustration of i) covalent bonding, ii) hydrogen bonding, and iii) π–π interaction in CDA-PAM hydrogel. c) Applications of CDA-PAM hydrogel-based TENG e-patch for promotion of wound healing, the inset shows the structure of the TENG-based e-patch.

difficult to assist to repair the wound in a timely and effective way. Recent developments in wearable and flexible bioelectronics with the advantages of light weight and ease of use provide a promising approach to solving this problem.[14] Especially, self-powered devices using flexible and wearable triboelectric nanogenerators (TENGs) brings new possibilities for ES-mediated skin regeneration.[15] These TENGs can be driven by normal human activities to generate electrical pulses through the combination of triboelectrification and electrostatic induction.[16–19] When used as a self-powered and wearable bioelectronic device, TENG offers unique advantages such as easy fabrication,[20,21] flexible working modes,[22,23] high energy conversion rate,[24] and is promising for providing *in-situ* ESs to effectively accelerate skin wounds.[25] Currently, there are several major problems that still need further improvement. First, traditional TENGs made of dielectric materials and metal electrodes are often rigid and mechanically mismatching with soft skin, thus difficult to be directly applied on wounds. Second, single-mode ES is still insufficient for promoting healing process of the wound. The combination of ESs with other pro-healing method is highly desired. Third, the therapeutic effect of ES is difficult to be monitored in a real-time manner, making the therapeutic schedule and decision delaying behind.

Recently, hydrogels have become emerging flexible materials for fabricating flexible TENGs due to their excellent stretchability,[26,27] good biocompatibility,[23] tissue conformability, and tunable conductivity.[27–29] The properties of the hydrogels can be rationally tailored by introducing appropriate fillers into the polymeric matrix, which enables the hydrogels to be suitable for fabricating TENG adaptive to various biomedical applications. The fillers with unique physicochemical properties can also endow the hydrogels with various performance, such as photothermal conversion effect that has potential to promote wound healing.[30–33] Based on these, we hypothesized that the functional hydrogel-based TENG can directly deliver ES and photothermal stimulation to the skin would for achieving better pro-healing results.[12,34] Concurrently, the local change of microenvironment that reflects healing process and therapeutic response can be monitored by the TENG in real-time, thereby facilitating the adjustment of the treatment plan in time.

Herein, we developed a flexible triboelectric wound e-patch to promote wound closure and capture electrical signals during healing process. This flexible patch can be used as a multifunctional sensor to detect various human movements including touch, bending and face recognition. In a rodent model of full-thickness dorsal skin wounds, this multifunctional, flexible e-patch can provide self-powered ES through the movement of mice. Furthermore, under the irradiation with a near-infrared (NIR) laser, it can provide photothermal effect rapidly to promote the regeneration of blood vessels. Under this combined therapeutic effect, the wounds closed completely after 14 days of treatment. The integration of sensor functions and therapeutic promotion capacity into a multifunctional, flexible TENG e-patch offers a new avenue for personalized healthcare electronics in diagnostic and therapy.

2. Results and Discussion

Scheme 1a,b displays the preparation process and chemical structure of the polyacrylamide (PAM) and polydopamine (PDA) based dual-network hydrogel doped with multi-walled carbon nanotubes (MCNTs). When the monomers of acrylamide (AM) and dopamine (DA), the filler carboxylated MCNTs, the initiators of ammonium persulfate (APS), N, N'-methylene bisacrylamide (BIS) and *N*,*N*,*N*′,*N*′-tetramethylethylenediamine (TEMED) are evenly mixed, the PAM and PDA chains crosslink randomly, physically, and covalently via the Schiff base reactions (Scheme 1b-i),[30,35] forming a PDA-PAM dual polymeric network, which is named as DA-PAM hydrogel. Within this dual network, the doped MCNTs improve the mechanical properties of the crosslinked network through the hydrogen bonding between —COOH groups of MCNTs and the $-NH_2$ groups of DA and the π–π interaction between DA (Scheme 1b-ii,iii). The obtained MCNTs doped hydrogel was named as CDA-PAM hydrogels. The electronic signals are generated when other materials contact and move away from the E-patch. Besides, MCNTs can also improve the electron conductivity of the hydrogel and provide the photothermal therapeutic effect under the NIR light irradiation, which might synergize with the ES for accelerating wound healing (Scheme 1c). During the therapy, the TENG can also monitor the temperature fluctuation at wound sites, providing a feedback of the therapeutic process.

We investigated the morphology, transparency, conductivity, mechanical strength, and adhesion properties of the as-prepared hydrogel. First, we tuned the amount of MCNTs in the hydrogel, and CDA1-PAM, CDA2-PAM, CDA3-PAM, and CDA4-PAM referred to the hydrogels doped with 0.5 mg MCNTs, 1.0 mg MCNTs, 1.5 mg MCNTs, and 3.0 mg MCNTs, respectively. From the scanning electron microscopy (SEM) image, CDA3-PAM hydrogel consisted of a 3D network with pore sizes varying from 10 to 50 µm (**Figure** 1a). The existence of MCNTs in CDA3-PAM increased the optical absorbance of the hydrogels particularly within the NIR light region, which was beneficial for photothermal conversion (Figure 1b; Figure S1, Supporting Information). Additionally, the conductivity of the hydrogels was obviously increased with increasing MCNT contents from 0.5 to 1.5 mg, however, dramatically decreased when the MCNTs content further increased to 3 mg, as shown in the current–voltage (*I-V*) curves in Figure 1c. We deduced that excessive MCNTs resulted in the aggregation of MCNTs in the hydrogel, leading to a discontinuous conductive network. Therefore, CDA3-PAM was chosen in the following experiments. The prepared CDA3-PAM displayed self-adhesive properties on various substances including plastic, glass, rubber, steel, and so on (Figure 1d). CDA3-PAM hydrogel showed satisfactory mechanical property and the doping of MCNTs led to unconspicuous variation of maximum tensile strength (0.9 MPa) and obvious increase of tensile strain (1165%) (Figure 1e,f). We further demonstrated the high conductivity and stretchability of the CDA3-PAM hydrogel by using it as a conductor in a circuit to light up a light-emitting diode (LED) bulb. As the CDA3-PAM hydrogel stretched, the LED light gradually became dimmed (Figure 1g). It was attributed to that stretching of the CDA3-PAM hydrogel induced an increase in its resistance, resulting in an elongated ion transmission pathway. The hydrogel displayed repeatable resistance fluctuations of up to ≈50% upon compression, indicating its sensitivity toward external force. (Figure 1h). The results in Figure 1i showed the strain-dependent resistance variation under stretching. The resistance varied timely and repeatedly with stretching, indicating a good sensitivity and stability.

Subsequently, the hydrogels were integrated with Ecoflex to form a single-electrode mode TENG (**Figure** 2a), in which Ecoflex was used as the contact triboelectric layer and the hydrogels acted as the electrode layer. The basic working mechanism and electrical output performance of the TENG are shown in Figure 2b–e. The as-prepared TENG works based on the coupling between triboelectrification and electrostatic induction (Figure 2b). When a dielectric material such as Kapton contacts with the TENG, electrification occurs at the contact interface, and equal amounts of charges with opposite polarities are generated at the surfaces of the two layers (Figure 2b-i). During this process, the Kapton surface is positively charged because of the higher surface electron affinity of the silicone elastomer. After the Kapton moves away from the TENG, positive charges are generated in the hydrogels, accompanied by charge flow (Figure 2b-ii). When the Kapton is far from the TENG, the electron flow stops (Figure 2b-iii). As the Kapton approaches the TENG again, electrons flow back to the hydrogel layer through the external circuit (Figure 2b-iv). As this process is repeated between the electrification layer and the Kapton, a pulsed current is generated. Meanwhile, Figure 2c shows a simple finite element simulation conducted by COMSOL Multiphysics to observe the potential distribution at different states. In addition, Figures 2d–e and S2 (Supporting Information) show the output performance of the hydrogel-based TENGs with different MCNT contents under a frequency of 1 Hz. A Kapton film (20 mm × 40 mm) was used as the triboelectric layer to contact with the Ecoflex layer of the TENGs. When the pure DA-PAM hydrogel was used as the electrode of the TENG, the TENG produced a V_{oc} output of 51.23 V, an I_{sc} of 1.23 µA, and a Q_{sc} of 26.23 nC, respectively. With increasing doping contents of MCNTs (0.5, 1, and 1.5 mg) in the hydrogels, the output of the TENGs increased gradually. However, as the doping of MCNTs was further increased to 3 mg (CDA4-PAM), the output of the TENG decreased back. The TENG made from CDA3-PAM hydrogel showed the highest output of 128.96 V, 1.79 µA, and 51.38 nC. This changing tendency was coincided with that of the hydrogel conductivity, where CDA3-PAM exhibited the highest conductivity (Figure 1b). In addition, the long-term stability of the TENG was investigated. It is found that the open-circuit voltage kept stable over 2000 cycles (Figure S3, Supporting Information).

Besides, when the TENG device was continuously stretched by four times to strains ranging from 0% to 300%, the resistance variation of the TENG followed a uniform pattern, indicating the highly sensitive and stable responses to the strains (Figure 2f). The V_{oc} increased as stretching strains increased from 0–300%, due to the coupling effect of the decreased dielectric layer's thickness and the increased contacting surface area according to the Poisson's effect (Figure S4, Supporting Information), which was

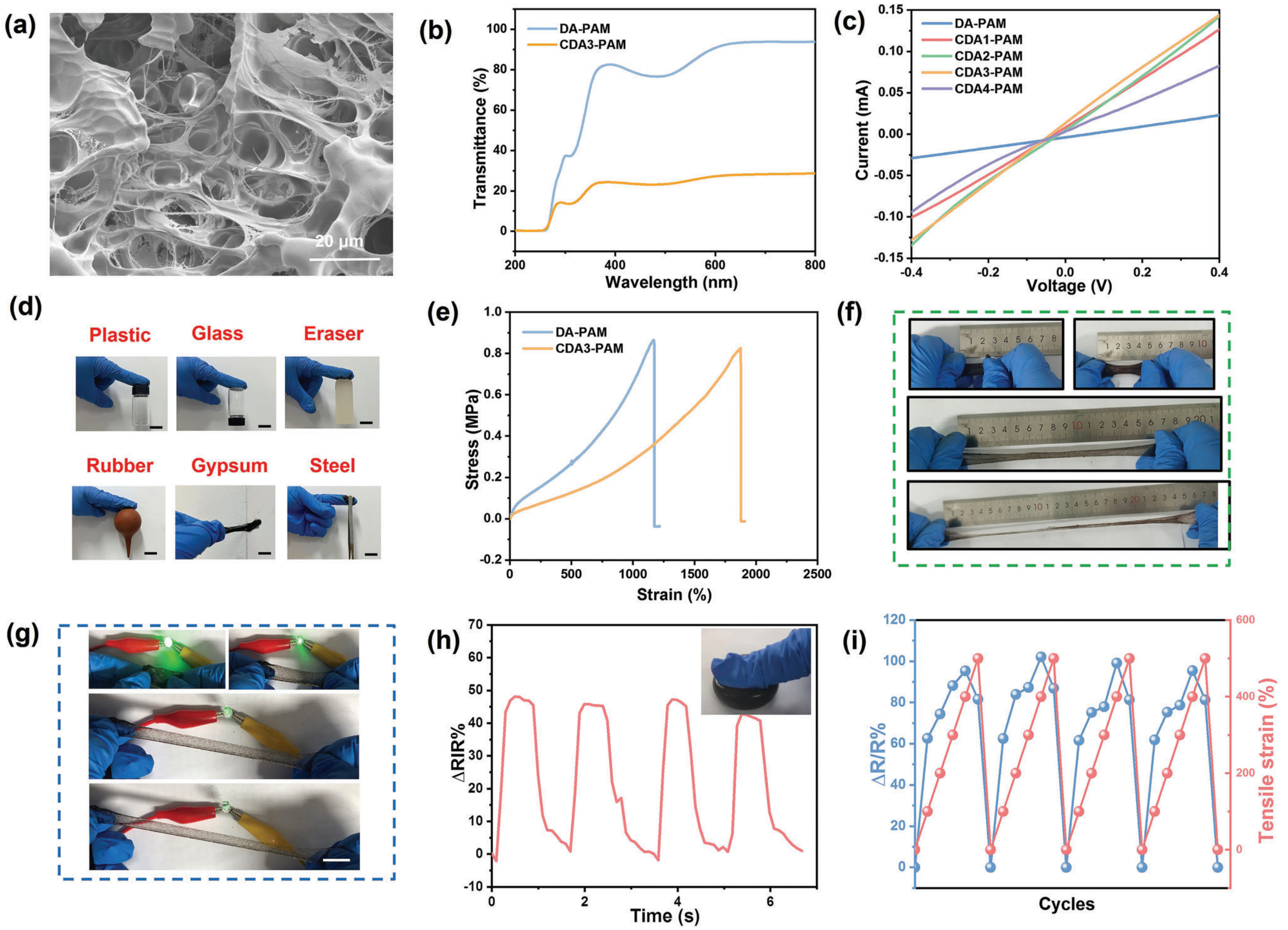

Figure 1. Characterization of the CDA3-PAM hydrogel. a) SEM image showing the morphology of the CDA3-PAM hydrogel. b) The UV–vis–NIR absorption spectra of the DA-PAM and CDA3-PAM hydrogels. c) Conductivity of the hydrogels with different contents of MCNTs. d) Adhesion demonstration of the CDA3-PAM hydrogel on different substrates. e) Stress-strain curves of the DA-PAM and CDA3-PAM hydrogels. f) Digital photographs of the CDA3-PAM hydrogel during stretching. g) Digital photographs of the stretched CDA3-PAM hydrogel in a conductive loop with a lightened LED bulb. h) Relative resistance changes under cyclic compression of the CDA3-PAM hydrogel. Inset photograph shows the compression progress. i) Relative resistance changes of the CDA3-PAM hydrogel under cyclic loading with strain of 0–500%. Scale bars in g and h represents for 1 cm.

in line with previous report.[36] Then, the sensitivity of the TENG was investigated (Figure 2g). When a finger touched the CDA3-PAM-based TENG, a fast response time (45 ms) and recovery time (60 ms) were observed, ensuring its timely sensing. Besides, long term repeatable cycles of the response and recovery times of the TENG was measured (Figure S5, Supporting Information). During 200 working cycles, the TENG displayed a stable response and recovery time, indicating the excellent response stability Therefore, the TENG made from CDA3-PAM hydrogel with the highest output performance was applied for the subsequent investigation unless specially mentioned. Additionally, to prove the reliability of the TENG in energy harvesting, resistors were employed as external loads to evaluate the output performance of TENG. According to Ohm's law, when the resistance of external load increased, the output voltage of the TENG gradually increased from 0, and the output current gradually decreases to 0 as shown in Figure S6a (Supporting Information). The output power density first increased with the increase of resistance value, then decreased. The TENG can reach to the maximum output power density of 81.86 mW m^{-2}, when the resistance value of external load is 100 MΩ, (Figure S6b, Supporting Information). As shown in Figure 2h, with the increasing of the capacitance of the capacitors, the charging speed gradually slowed down and the charging time was prolonged. Within 60 s at 1 Hz, a 1 μF capacitor can be rapidly charged to 3.3 V by the developed TENG, while the 2.2 μF one can be charged to 2.8 V. Therefore, the TENG exhibited excellent universality of charging capacity for different capacitors.

The appearance of wounds may disrupt the skin's capacity of sensing external stimuli, e.g., pressure and touch. The wearable TENG as an e-patch is expected to be capable of compensating for these temporary difficulties through its electromechanical signal transitions during stretching or deforming. As displayed in **Figure 3**, the CDA-PAM-based TENG can be utilized as either a piezoresistive sensor or a self-powered biomechanical sensor for monitoring human's normal activity in a variety of scenarios. As displayed in Figure 3a, the TENG's variation in $\Delta R/R_0$ allowed us to clearly distinguish the finger actions of touch, tap, and press

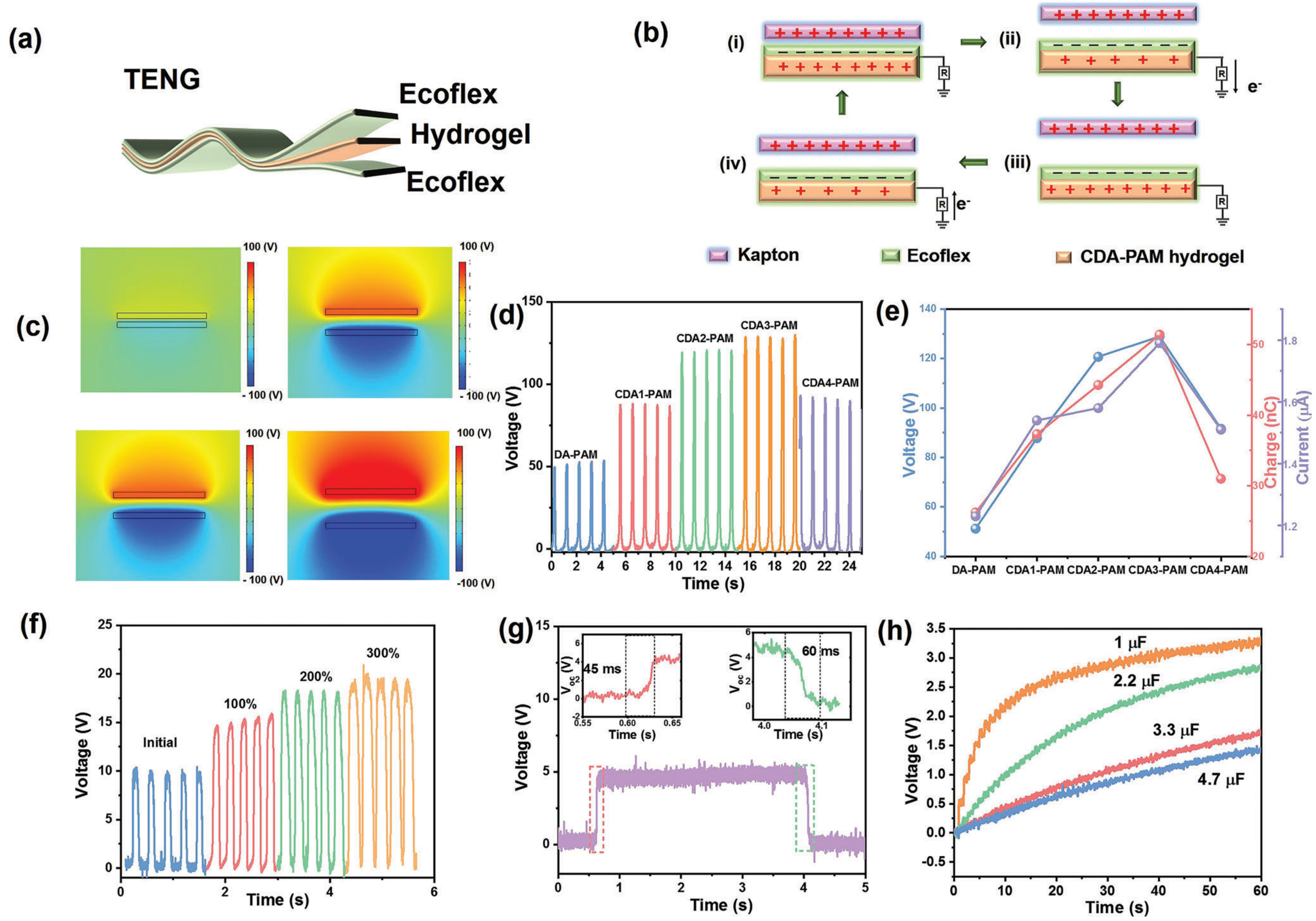

Figure 2. Characterization of the hydrogel-based TENG. a) Schematic diagram of the hydrogel-based TENG. b) Working mechanism of the hydrogel-based TENG. c) Simulation of the potential distribution of the hydrogel-based TENG by COMSOL Multiphysics. d) Open-circuit voltage (V_{oc}) output of the TENG made from the hydrogels with different MCNT doping. e) The output comparison of the TENG made from the hydrogels with different MCNT doping. f) V_{oc} output of the TENG (1 × 1 cm) at different stretching ratios. g) Response time of the TENG under finger tough. h) Charging voltage curves of different commercial capacitors (1, 2.2, 3.3, and 4.7 μF) by the TENG.

with different pressures. Similarly, the TENG could also detect the bending angle of fingers (Figure 3b). Based on its multifunctionality, the TENG is capable of monitoring human movement in real-time, recognizing the mouth open and blowing precisely (Figure 3c,d). In another scenario, the TENG sensor could monitor frown of the user (Figure 3e) in its voltage output mode. In a same manner, the cyclic wrist bending could be effectively monitored and presented in the form of output voltage signals, in which the peak voltage value varied with the bending angles. As the bending angles increased from 30° to 90°, the peak output voltage increased from 5 to 17 V accordingly, which was due to the increased contact area between Ecoflex and the skin at a larger bending angle (Figure 3f). The TENG can be attached to the neck to detect small deformations of skin and muscle. When the volunteer raised or lowered his head, the neck movements could be precisely monitored (Figure 3g). The real-time signals generated by the TENG attached to the knee were also measured to monitor the bending and release of the knee (Figure 3h). Therefore, the flexible and stretchable TENG with high sensitivity and good repeatability demonstrated potentials for real-time and self-powered biomechanical sensing.

As a smart wearable sensor, the wearable TENG as an e-patch had excellent photothermal conversion properties, which can synergize with the ES to promote wound healing. **Figure 4a** illustrated the process of wound healing by the combination of ES and photothermal effect. When irradiated with NIR light, the temperature of the TENG can quickly increase due to the existence of MCNTs, a typical photothermal conversion material. The local heat can accelerate microcirculation of blood flow and relieve pain in the injured site, and ES can facilitate the migration, proliferation, and differentiation of wound repair cells such as fibroblasts.[37] The photothermal conversion of the DA-PAM hydrogel, CDA3-PAM hydrogel, and CDA3-PAM-based TENG were recorded under the NIR laser irradiation (808 nm, 0.5 W cm^{-2} with distance of 4 cm). And according to the results in Figure 4b, it showed that the surface temperature of the CDA3-PAM hydrogel rapidly increased to 53.8 °C after 5 min of irradiation, while the surface temperature of the CDA3-PAM-based TENG was 46.1 °C. In contrast, the surface temperature of DA-PAM hydrogel only had a slight temperature increase to 28.5 °C. These results indicated that the doping of MCNTs endowed excellent photothermal properties to the CDA3-PAM hydrogel and the

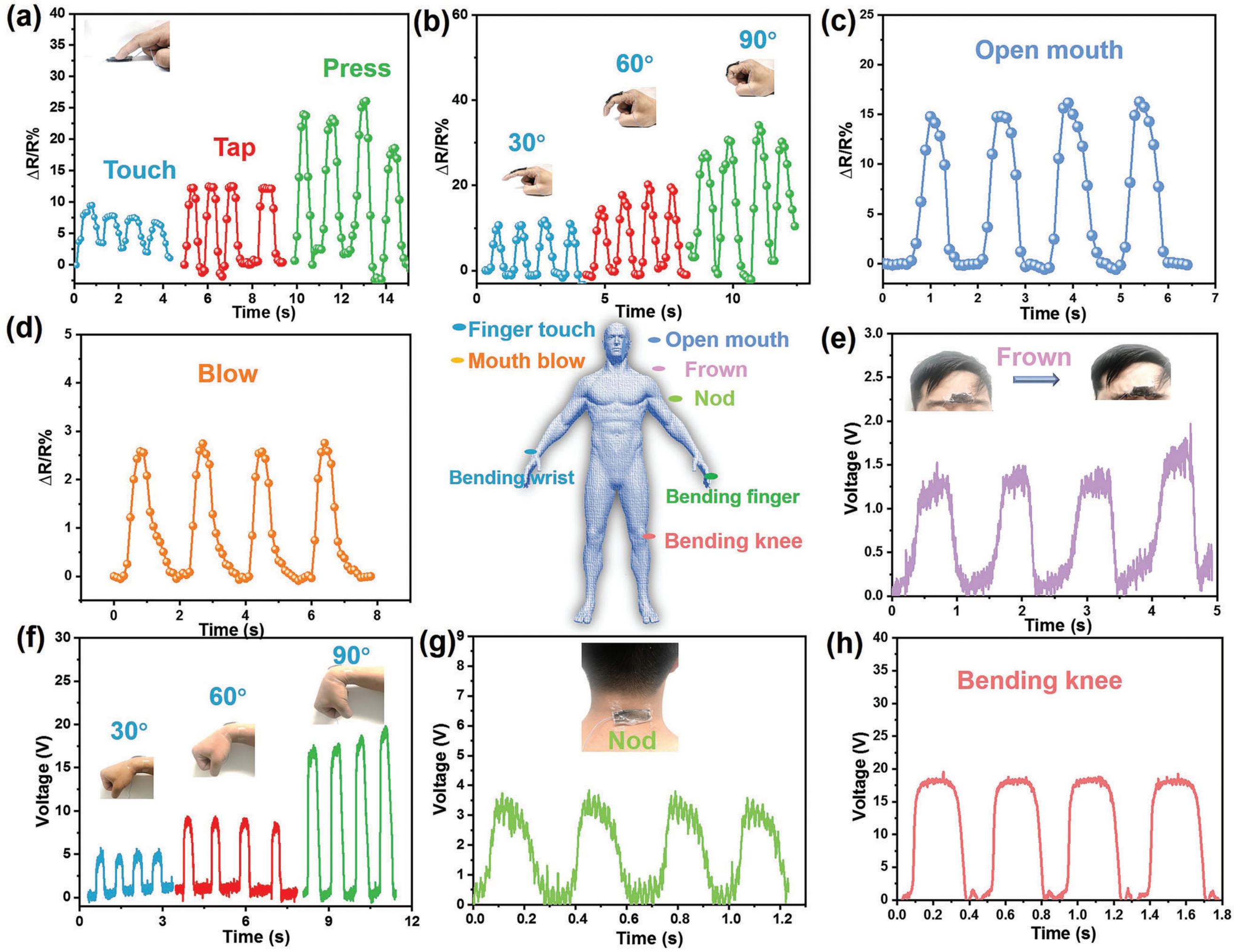

Figure 3. Biomechanical sensing of normal human activities with the self-powered TENG sensor. Relative resistance changes for real-time monitoring of a) different contact strengths of a finger, b) finger bending, c) mouth open, and d) blow. Voltage outputs as a self-powered TENG sensor for sensing e) frown, f) wrist bending, g) neck movement, and h) knee bending.

encapsulation of CDA3-PAM hydrogel with Ecoflex slightly decreased its photothermal conversion. This is helpful for avoiding burning of the skin around the wound within a short time, and after 5 min irradiation, the local temperature rose to 46.1 °C, which can accelerate the blood circulation. A similar trend was also displayed in the infrared images of Figure 4c. This photothermal conversion can be repeated under the repeated light irradiation (Figure 4d).

Next, we measured the photocurrents of CDA3-PAM and DA-PAM hydrogels generated under full-spectrum light irradiation and the results demonstrated that CDA3-PAM could generate a photocurrent of 0.25 μA, significantly higher than 0.05 μA of the DA-PAM hydrogel (Figure 4e). Another interesting phenomenon is that the temperature change of the TENG can be reflected by the change in the resistance of the hydrogel. This property endowed the TENG with the capability to monitor the temperature fluctuation at wound sites during healing process, which is closely related to inflammation, infection, blood supply, etc.[37] To validate the capacity of the TENG to sense temperature change, the TENG e-patch was attached to a pig skin, and the change rate of resistance along with the local temperature changes were recorded. As shown in Figure 4f, the resistance change rate $\Delta R/R\%$ of the TENG increased when the surface temperature increased from 25 to 45 °C, and $\Delta R/R\%$ decreased when the surface temperature decreased again, indicating the temperature-sensing capability of the TENG (Figure 4f).

Based on the integrated properties including self-powered electrical generation to provide local ES, photothermal conversion capacity and high biocompatibility, we utilized the hydrogel-based TENG as a flexible e-patch to accelerate wound healing in a rodent model of full-thickness dorsal skin wound. Before conducting in vivo experiment, the biocompatibility of the hydrogel with different contents of MCNTs and the Ecoflex have been investigated. The live/dead cell viability staining results showed that all of these materials exhibited excellent biocompatibility (Figure S7, Supporting Information). In addition, we confirmed that electrostimulation could effectively promote cell migration by the cell scratching assay (Figure S8, Supporting Information).

NANO · MICRO small
www.small-journal.com

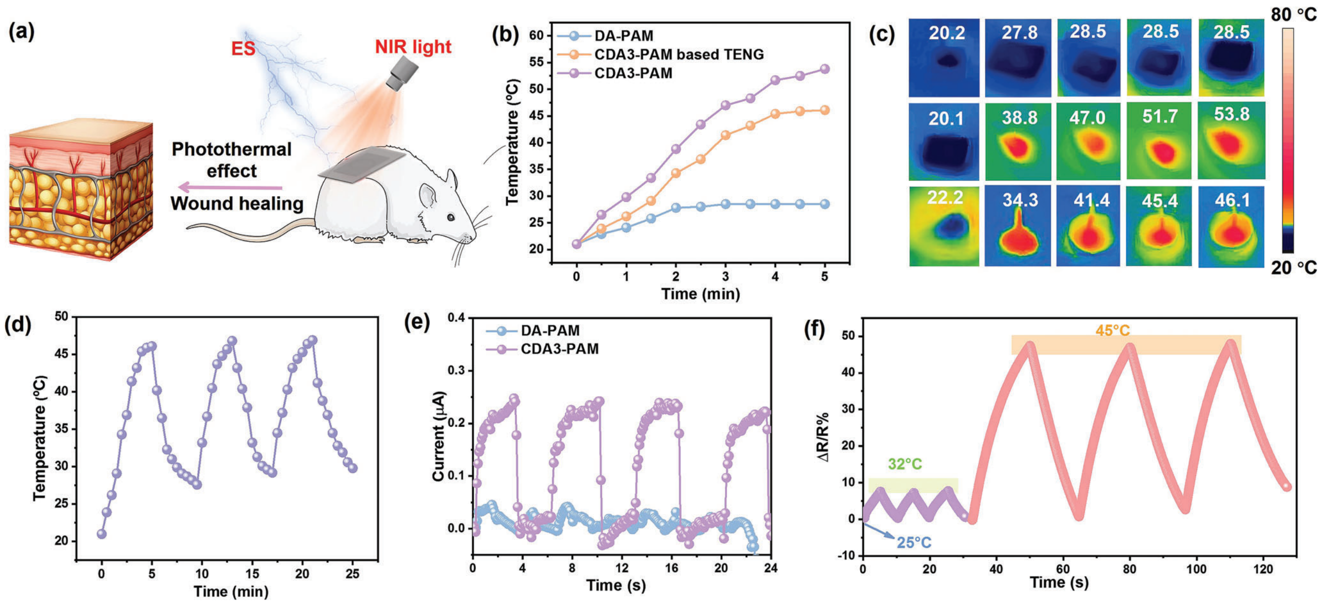

Figure 4. Photothermal conversion and temperature-sensitive properties of the TENG. a) Illustration of the wound healing process with the synergy of ES and photothermal effect. b) Photothermal conversion curves of DA-PAM hydrogel, CDA3-PAM hydrogel, and CDA3-PAM based TENG under NIR light irradiation (0.5 W cm^{-1} with distance of 4 cm). c) Infrared images of the above samples under NIR laser irradiation. d) Surface temperature changes of the CDA3-PAM hydrogel under repeated NIR laser irradiations. e) Time-dependent photocurrent density of the DA-PAM, and CDA3-PAM hydrogels under full-spectrum light irradiation. f) Continuous monitoring of the resistance of CDA3-PAM hydrogel under temperature fluctuations (25–32 and 25–45 °C) on the pigskin surface.

Mice with full-thickness dermal wounds (10 mm in diameter) were randomly divided into six groups ($n = 5$), including Control group, NIR laser irradiation group (L), TENG e-patch group without external output electrode (TENG), TENG plus near-infrared light irradiation group (L + TENG), TENG e-patch with external output electrode (TENG-E), and TENG e-patch with external output electrode plus near-infrared light irradiation group (L + TENG-E). The wounding and administration were illustrated in **Figure** 5a that the e-patches were covered on the wounds with the assistance of medical tape and changed for every three days. The local NIR light irradiation was imposed on days 0, 2, 5, 8, and 11. After the 14-days of treatment period, the therapeutic outcome was evaluated, and the main tissues were harvested for pathological study. When the TENG e-patch was adhered on the surface of the wounds, the normal activities (breathing, trembling, crawling, etc.) of mice drove the production of local triboelectric voltages reaching 0.1 ≈ 0.23 V (Figure S9, Supporting Information). After the therapy, the L + TENG-E group with simultaneous photothermal and electrical stimulation had the superior pro-healing effect (Figure 5b–e). At day 2, the wounds in the L + TENG-E group were reduced by ≈30% with the formation of scabs, and the wounds were almost closured on day 14. The wound healing rates of the TENG-E and L+TENG groups were also higher than those of the control group on day 14, and the healed areas of the mice wounds were ≈84.1% and 85.9%, respectively. The control group without any treatment had a relatively poor healing rate, and the scabs appeared until day 8 and ≈25.9% of the dermis remained unhealed on day 14. At the end of the treatment, there was no significant difference in the body weight of the mice in each group, suggesting high compatibility of the therapeutic process (Figure 5d).

To verify the effectiveness of synergistic photothermal and local ES on dermal tissue regeneration, histological assessment of the dermal tissues after the treatments was performed using hematoxylin and eosin (H&E), Masson's trichrome, and immunohistochemical staining of tumor necrosis factor-α (TNF-α) and platelet endothelial cell adhesion molecule-1 (CD31). The H&E-stained dermal tissue in Figure 5f displayed that the L + TENG-E group had the most intact dermal tissue integrity, epithelialization, and the smallest wound width. In addition, collagen deposition is a crucial marker of tissue remodeling, which increases tissue strength and creates a favorable environment for cell migration and proliferation. Masson trichrome's staining was used to analyze the collagen deposition in the wound dermis and the results suggested that there existed significantly more newly generated and ordered deposited collagen fibers in the regenerated dermis of the L + TENG-E group (Figure 5f). As illustrated in Figure S10 (Supporting Information), under the synergistic effect of photothermal and electrical stimulation, collagen deposition reached 69.09% and the collagen displayed a well-organized arrangement. In contrast, the collagen-positive area in the control group was only 33.84%. Moreover, we can observe many neogenic hair follicles in the regenerated area in the L+TENG-E group, indicating that the synergistic effect of photothermal and ES favors trauma repair (Figure 5f; Figure S11, Supporting Information). During healing process, TNF-α and CD31 are important biomarkers reflecting inflammation and vascular regeneration, respectively. From the immunohistochemical results (Figure 5g–j), on day 2, L + TENG-E group showed the least TNF-α expression Day 2; after 14 days of treatment, the L + TENG-E group had the highest expression of CD31, indicating that the synergistic effects of ES and photothermal effect

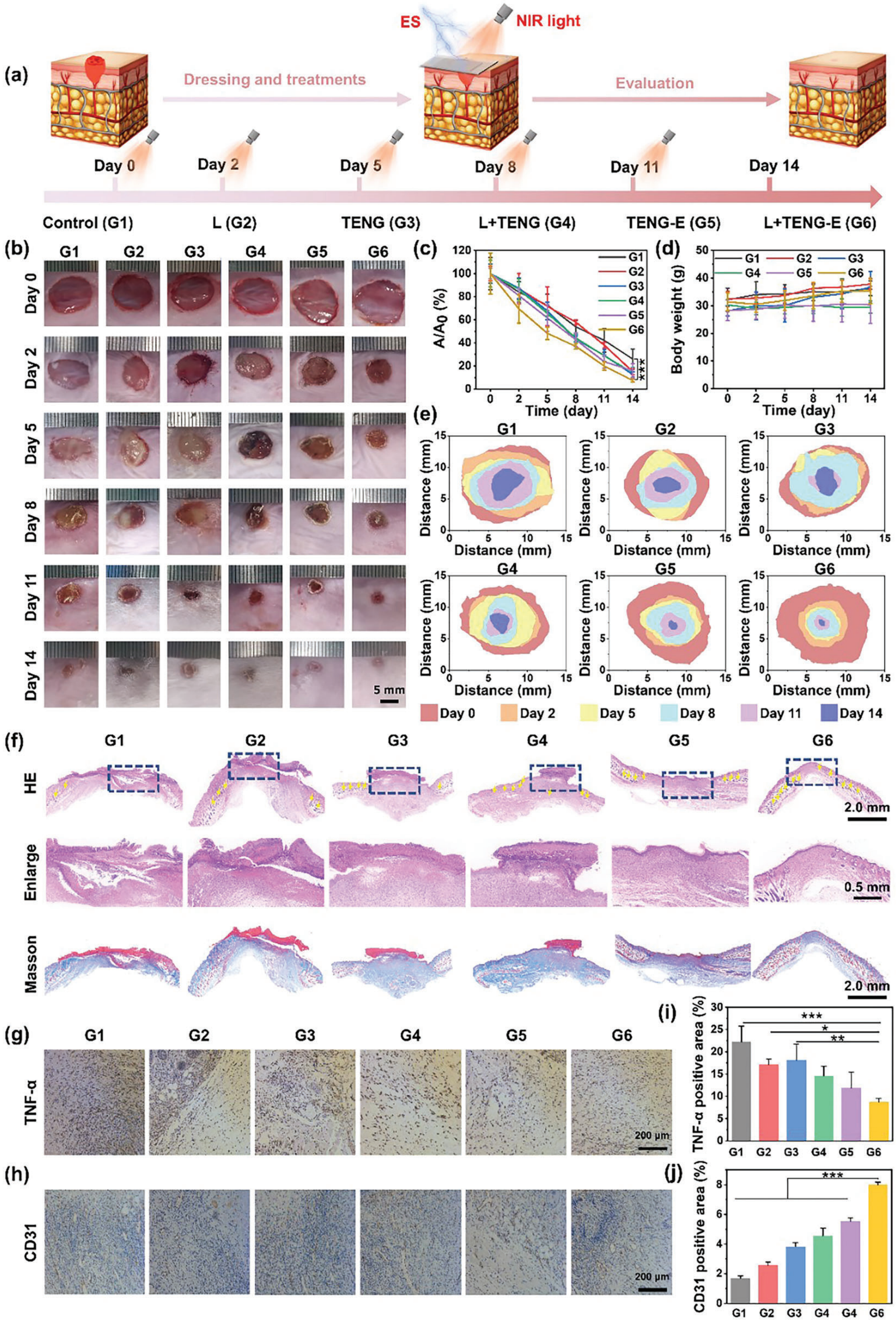

Figure 5. TENG as an e-patch for the promotion of wound healing in mice through the synergy of ES and photothermal effect. a) Schematic and timeline of the full-thickness dermal wound healing therapeutic process. b) Representative optical images of the wounds during the therapy. c) Relative wound area of different groups during the therapy. d) Body weight change of the mice during the therapy. e) Wound closure traces of the mice. f) H&E staining and Masson's trichrome staining of the tissue sections extracted from the wound area on day 14 (Yellow arrows indicate new hair follicles). Immunohistochemistry of g) the inflammatory factor TNF-α on day 2 and h) the vascular regeneration factor CD31 on day 14. Quantification analysis of i) TNF-α and j) CD31 positive area.

can efficiently reduce inflammation and promote vascular regeneration. Additionally, no obvious inflammatory lesions or tissue damage were observed in the main organs including the heart, liver, spleen, lung, or kidney of all mice (Figure S12, Supporting Information). These results suggested that the ES and photothermal stimulation using the hydrogel-based TENG e-patch had great potential in accelerating wound healing with obvious pro-healing effect and good biocompatibility.

3. Conclusion

In conclusion, we have successfully fabricated a flexible and temperature-sensing triboelectric e-patch (CDA-PAM-based TENG) for accelerating wound healing with the synergy of ES and photothermal effect. The multifunctional CDA-PAM hydrogel used to fabricate the e-patch has the advantages of high flexibility, stretchability, conductivity, and biocompatibility. It can be applied as the electrode of the TENG to harvest energy or sense human activities and the temperature fluctuation of wound sites, as well as promote the healing process of skin wounds. This work contributes to the development of an integrated e-patch in wound management and monitoring.

4. Experimental Section

Chemicals: MCNTs, AM, DA, TEMED, BIS and APS were purchased from Macklin and used without purified. Fresh pigskin was bought from the supermarket and cleaned with ethanol.

Synthesis of the DA-PAM and CDA-PAM Hydrogels: For the fabrication of the CDA-PAM hydrogels, 3.0 g AM was dissolved in 10 mL H_2O, MCNTs (0.5, 1, 1.5, or 3 mg) and 3 mg DA were added and mixed. And then 15 mg APS and 6 mg BIS were added under stirring for 5 min. Finally, 20 µL TEMED was poured into the above solution and stirred for seconds. The mixture was transferred into a culture dish for polymerization to produce the final CDA-PAM hydrogels, namely CDA1-PAM (0.5 mg MCNTs), CDA2-PAM (1 mg MCNTs), CDA3-PAM (1.5 mg MCNTs) and CDA4-PAM (3 mg MCNTs), respectively. The synthesis of the DA-PAM hydrogel was similarly to the CDA-PAM hydrogels without the addition of MCNTs.

Characterization: The morphology and structure of the hydrogel were characterized by SEM (Hitachi, SU-8020). The UV–vis–NIR absorbance spectra were acquired on a Shimadzu UV-3600 spectrophotometer. The triboelectric output of TENGs were recorded using a Keithley 6514 electrometer. The performances of all the hydrogels as piezoresistive sensors were measured using an electrochemical workstation (CH 660E, China). The change of relative resistance was calculated according to $\Delta R/R \times 100\%$, in which $\Delta R = R - R_0$, where R was the dynamic resistance under different strains, and R_0 was the resistance at the initial state without strain.

Cellular Biocompatibility: CDA-PAM hydrogels with different carbon nanotube contents were soaked in 75% ethanol for 6 h, and then washed with sterilized deionized water three times for 10 min each to wash away the uncross-linked acrylamide. The biocompatibility of the material was then determined by the leaching method. 1 g of CDA-PAM hydrogel was immersed in 10 mL of DMEM containing 10% fetal bovine serum and 1% penicillin-streptomycin solution for 24 h at 37 °C, 5% CO_2. Mouse fibroblasts (L929) were inoculated in 24-well plates at a density of 5×10^4 per well. After the cells were adhered to the wall, the culture medium was changed to the extraction solution, and after 24 h of incubation, live-dead staining was performed using the live-dead staining kit purchased by Service-bio, the staining steps were referred to the instruction manual. Finally, the survival of the cells was observed by fluorescence confocal.

Cell Migration: Cells were inoculated in 6-well plates at a density of 5×10^4 cells per well and incubated for 12 h. After the cells reach confluence, a straight line was drawn in the middle of each well with a sterilized 10 µL pipette tip. The cells were then washed twice with cell culture medium to remove detached cells. Electrodes were inserted to both sides of the scratch and powered using TENG for 10 min each time at 0 and 12 h. Cell migration was monitored by light microscopy after 0, 12, and 24 h of co-culture.

In Vivo Wound Healing: The mice were provided by Charles River Laboratories, Beijing, and the animal handling procedures strictly complied with the national standard "Requirements for Laboratory Animal Environment and Residence Facilities (GB 14925-2001)," and the animal experiments were approved by the Ethics Committee of Beijing Institute of Nanoenergy and Nanosystems (Approval Number: 2023A036). Female ICR mice (≈30 g) were randomly divided into six groups: i) Control group, ii) L group, iii) TENG group, iv) L+TENG group, v) TENG-E group, and vi) L + TENG-E group. Note that in this part, TENG group means the wound was covered with the e-patch and did not applied with the output electrode. After anesthetized with 4% chloral hydrate, the dorsal hair of the mice was removed with the depilatory cream, and a full-thickness circular wound with a diameter of ≈10 mm was made on the back of each mouse under aseptic conditions. Specifically, the wounds in the Control group remained untreated. The wounds in the NIR-involved groups were subjected to NIR laser irradiation (808 nm, 0.5 W cm^{-2}, 5 min) on days 0, 2, 5, 8, and 11. The wounds in the TENG-involved groups were completely covered with the TENG e-patches (square shape, 2 cm × 2 cm, hydrogel diameter of 1.5 cm). And the wounds in the ES-involved groups were TENG-E and L + TENG-E. All the e-patches were adhered onto the wound with the assistance of transparent medical tape, and wounds in all groups were photographed and the healing rates were calculated as a percentage of the original wound area assessed using ImageJ software. In addition, wounds from all groups were collected for histological analysis.

Histopathological Analysis and Immunohistochemical Staining: The regenerated skin was dissected and collected from all groups after 2 and 14 days of treatment. After fixation with 4% paraformaldehyde at 4 °C for 24 h, the tissue specimens were embedded in fused paraffin and serially cut into 4 µm thick sections. Samples were used for hematoxylin and eosin (H&E) or Masson's trichrome staining and observed under a light microscope to assess tissue regeneration, epithelialization, inflammatory level, neovascularization, and collagen deposition. Immunohistochemical assessment of TNF-α and CD31 was performed using the appropriate monoclonal antibodies (Servicebio) according to the protocol provided by the manufacturer. The stained sections were observed and TNF-α and CD31 positive areas were measured using Image J.

Statistical Analysis: All the experiments were performed with sample sizes more than three, and the experimental results were expressed as the mean value ± standard deviation. The difference between groups was determined using a one-way analysis of variance (ANOVA), and the p value less than 0.05 was considered statistically significant ($^{*}p < 0.05$, $^{**}p < 0.01$, $^{***}p < 0.001$).

Supporting Information

Supporting Information is available from the Wiley Online Library or from the author.

Acknowledgements

Z.W. and Q.H.H. contributed equally to this work. The work was supported by the National Natural Science Foundation of China (Nos. 82072065 and 22205260), the Strategic Priority Research Program of the Chinese Academy of Sciences, China (No. XDA16021103), the Fundamental Research Funds for the Central Universities (E2EG6802X2), and the National Youth Talent Support Program, China.

Conflict of Interest

The authors declare no conflict of interest.

Data Availability Statement

The data that support the findings of this study are available from the corresponding author upon reasonable request.

Keywords

electrical stimulation, hydrogel, self-powered, triboelectric nanogenerator (TENG), wound healing

Received: October 22, 2024
Revised: December 2, 2024
Published online:

[1] B. Guo, R. Dong, Y. Liang, M. Li, *Nat. Rev. Chem.* **2021**, *5*, 773.
[2] M. Kurita, T. Araoka, T. Hishida, D. D. O'Keefe, Y. Takahashi, A. Sakamoto, M. Sakurai, K. Suzuki, J. Wu, M. Yamamoto, R. H. Benitez, A. Ocampo, P. Reddy, M. N. Shokhirev, P. Magistretti, E. N. Delicado, H. Eto, K. Harii, J. C. I. Belmonte, *Nature* **2018**, *561*, 243.
[3] W. Li, Y. Yu, R. Huang, X. Wang, P. Lai, K. Chen, L. Shang, Y. Zhao, *Adv. Sci.* **2023**, *10*, 2301479.
[4] C. Wang, X. Jiang, H. J. Kim, S. Zhang, X. Zhou, Y. Chen, H. Ling, Y. Xue, Z. Chen, M. Qu, L. Ren, J. Zhu, A. Libanori, Y. Zhu, H. Kang, S. Ahadian;, M. R. Dokmeci, P. Servati, X. He, Z. Gu, W. Sun, A. Khademhosseini, *Biomaterials* **2022**, *285*, 121479.
[5] Q. Hu, X. Wan, S. Wang, T. Huang, X. Zhao, C. Tang, M. Zheng, X. Wang, L. Li, *Sci. China Mater.* **2023**, *66*, 3347.
[6] C. Wang, E. Shirzaei Sani, C.-D. Shih, C. T. Lim, J. Wang, D. G. Armstrong, W. Gao, *Nat. Rev. Chem.* **2024**, *9*, 550.
[7] G. Yao, X. Y. Mo, C. H. Yin, W. H. Lou, Q. Wang, S. R. Huang, L. N. Mao, S. H. Chen, K. N. Zhao, T. S. Pan, L. Huang, Y. Lin, *Sci. Adv.* **2022**, *8*, eabl8379.
[8] R. Nazari-Vanani, M. Vafaiee, E. Asadian, R. Mohammadpour, H. Rafii-Tabar, P. Sasanpour, *Biomater. Adv.* **2023**, *149*, 213364.
[9] C. D. McCaig, A. M. Rajnicek, B. Song, M. Zhao, *Physiol. Rev.* **2005**, *85*, 943.
[10] Y. Liang, J. He;, *ACS Nano* **2021**, *15*, 12687.
[11] X. Chen, X. Xie, Y. Liu, C. Zhao, M. Wen, Z. We, *Adv. Funct. Mater.* **2020**, *30*, 04673.
[12] H. G. Menge, N. D. Huynh, K. Choi, C. Cho, D. Choi, Y. T. Park, *Adv. Funct. Mater.* **2022**, *33*, 10571.
[13] C. C. Víctor, A. Carlos, P. M. Maria, *Biomater. Sci.* **2023**, *11*, 2266.
[14] S. Guan, J. Li, Y. Wang, Y. Yang, X. Zhu, D. Ye, R. Chen, Q. Liao, *Adv. Mater.* **2023**, *35*, 2304465.
[15] F. R. Fan, Z. Q. Tian, Z. L. Wang, *Nano Energy* **2012**, *1*, 328.
[16] Z. Wang, Z. R. Liu, G. R. Zhao, Z. C. Zhang, X. Y. Zhao, X. Y. Wan, Y. L. Zhang, Z. L. Wang, L. L. Li, *ACS Nano* **2022**, *16*, 1661.
[17] W. Jiang, H. Li, Z. Liu, Z. Li, J. Tian, B. Shi, Y. Zou, H. Ouyang, C. Zhao, L. Zhao, R. Sun, H. Zheng, Y. Fan, Z. L. Wang, Z. Li, *Adv. Mater.* **2018**, *30*, 1801895.
[18] G. Zhao, Y. Zhang, N. Shi, Z. Liu, X. Zhang, M. Wu, C. Pan, H. Liu, L. Li, Z. L. Wang, *Nano Energy* **2019**, *59*, 302.
[19] X. He, H. Zou, Z. Geng, X. Wang, W. Ding, F. Hu, Y. Zi, C. Xu, S. L. Zhang, H. Yu, M. Xu, W. Zhang, C. Lu, Z. L. Wang, *Adv. Funct. Mater.* **2018**, *28*, 05540.
[20] L. Ma, R. Wu, S. Liu, A. Patil, H. Gong, J. Yi, F. Sheng, Y. Zhang, J. Wang, J. Wang, W. Guo, Z. L. Wang, *Adv. Mater.* **2020**, *32*, 2003897.
[21] Y. Hu, Z. Zheng, *Nano Energy* **2019**, *56*, 16.
[22] Y. Long, Z. Wang, F. Xu, B. Jiang, J. Xiao, J. Yang, Z. L. Wang, W. Hu, *Small* **2022**, *18*, 2203956.
[23] Z. Li, C. Li, W. Sun, Y. Bai, Z. Li, Y. Deng, *ACS Appl. Mater. Interfaces* **2023**, *15*, 12787.
[24] S. S. Kwak, S. M. Kim, H. Ryu, J. Kim, U. Khan, H. J. Yoon, Y. H. Jeong, S. W. Kim, *Energy Environ. Sci.* **2019**, *12*, 3156.
[25] Y. Long, H. Wei, J. Li, G. Yao, B. Yu, D. Ni, A. L. Gibson, X. Lan, Y. Jiang, W. Cai, X. Wang, *ACS Nano* **2018**, *12*, 12533.
[26] Y. Dou, Z. P. Wang, W. He, T. Jia, Z. Liu, P. Sun, K. Wen, E. Gao, X. Zhou, X. Hu, J. Li, S. Fang, D. Qian, Z. Liu, *Nat. Commun.* **2019**, *10*, 5293.
[27] H. He, H. Li, A. Pu, W. Li, K. Ban, L. Xu, *Nat. Commun.* **2023**, *14*, 759.
[28] X. Ren, M. Yang, T. Yang, C. Xu, Y. Ye, X. Wu, X. Zheng, B. Wang, Y. Wan, Z. Luo, *ACS Appl. Mater. Interfaces* **2021**, *13*, 25374.
[29] C. Lu, X. Chen, *Nano Lett.* **2020**, *20*, 1907.
[30] Y. Li, D. Yang, Z. Wu, F. L. Gao, X. Z. Gao, H. Y. Zhao, X. Li, Z. Z. Yu, *Nano Energy* **2023**, *109*, 108324.
[31] J. Wu, W. Wang, J. Shen, N. Zhou, Y. Li, B. Z. Tang, M. Zhang, *Adv. Funct. Mater.* **2024**, *34*, 2312374.
[32] M. Fu, Y. Zhao, Y. Wang, Y. Li, M. Wu, Q. Liu, Z. Hou, Z. Lu, K. Wu, J. Guo, *Small* **2023**, *19*, 2205489.
[33] Y. Wang, K. Liu, W. Wei, H. Dai, *Adv. Funct. Mater.* **2024**, *34*, 2402531.
[34] G. Guedes, S. Wang, F. Fontana, P. Figueiredo, J. Linden, A. Correia, R. J. B. Pinto, S. Hietala, F. L. Sousa, H. A. Santos, *Adv. Mater.* **2021**, *33*, 2007761.
[35] Y. Long, Y. Chen, Y. Liu, G. Chen, W. Guo, X. Kang, X. Pu, W. Hu, Z. L. Wang, *Nanoscale* **2020**, *12*, 12753.
[36] D. Yang, Y. Ni, X. Kong, S. Li, X. Chen, L. Zhang, Z. L. Wang, *ACS Nano* **2021**, *15*, 14653.
[37] M. Mao, J. Kong, X. Ge, Y. Sun, H. Yu, J. Liu, W. Huang, D. Y. Wang, Y. Wang, *Chem. Eng. J.* **2024**, *482*, 148949.